Quantitative attribution of the temperature associated with winter extreme cold events in China

Weiwei Wang[1,2] · Tuantuan Zhang[1,3] · Junwen Chen[4] · Qingquan Li[5] · Song Yang[1,3] · Yi Deng[6]

Abstract

Extreme cold events exert enormous impacts on the ecosystems and human health. A quantitative attribution analysis of the surface temperature anomalies associated with extreme cold events in China is conducted using an updated version of the coupled atmosphere-surface climate feedback response analysis method. For both extreme warm and cold years, the effects of anomalous surface albedo, water vapor, atmospheric dynamics, and aerosols are the major positive contributors, and the processes associated with surface dynamics provide a major negative effect. Specifically, the effect of surface albedo (water vapor) is directly linked to the change in local snow cover (precipitable water) over China. More local snow cover (precipitable water) provides a cooling (warming) effect and vice versa. The process associated with atmospheric dynamics exhibits an asymmetric contribution for the extreme warm and cold years. It provides a warming effect over most of China in the extreme warm years, which is possibly related to the nation-wide warm air advection. On the other hand, the effect of atmospheric dynamics displays large regional and year-to-year variations for the cold cases. In addition, a considerable impact of anthropogenic aerosols is detected over central-southern China, which is possibly related to the emission reduction policies in China since 2013. Although clouds show only a moderate impact on the national-averaged temperature anomalies, they provide a considerable effect over southern China.

Keywords Winter extreme cold events · Quantitative attribution · Radiative and non-radiative processes · China

✉ Tuantuan Zhang
zhangtt75@mail.sysu.edu.cn

✉ Song Yang
yangsong3@mail.sysu.edu.cn

[1] Southern Marine Science and Engineering Guangdong Laboratory (Zhuhai), School of Atmospheric Sciences, Sun Yat-Sen University, Zhuhai 519082, China

[2] Meteorological Bureau of Shenzhen Municipality, Shenzhen 518040, China

[3] Guangdong Province Key Laboratory for Climate Change and Natural Disaster Studies, Sun Yat-Sen University, Zhuhai 519082, China

[4] Shenzhen Wiselec Technology Co., Ltd, Shenzhen 518048, China

[5] China Meteorological Administration Key Laboratory for Climate Prediction Studies, National Climate Center, Beijing 100081, China

[6] School of Earth and Atmospheric Sciences, Georgia Institute of Technology, Atlanta, GA 30319, USA

1 Introduction

Extreme events have received increased research interest during the recent decades, given their devastating effects on human health and the ecosystems (McMichael 2013; Ebi and Bowen 2016; Cui et al. 2017; Harris et al. 2018; Raymond et al. 2020; Guan et al. 2022). In the context of global warming, the extreme cold events in China have increased remarkably after 2006 (Wang and Chen 2014a; Wang and Lu 2016; Chen et al. 2019, 2023; Fu and Ding 2021). For example, extraordinarily frequent and long-lasting snowstorms hit China in January 2008, with excessive snow amount, persistent low temperatures, and severe icing conditions over central and southern China (Wen et al. 2009; Zhou et al. 2009). Severely extreme cold events also occurred over China in the winters of 2011, 2016, and 2021 (Gong et al. 2014; Song and Wu 2017; Yu et al. 2022). Surface air temperature was observed more than 10 °C lower than the historical average in some parts of China during 20–25 January 2016 (Song and Wu 2017), and the new record-breaking low

temperatures reached – 19.6 °C and – 19.9 °C in Beijing and Tianjin on 7 January 2021, respectively (Zhang et al. 2022b).

The interannual variability of extreme temperature is regulated by both atmospheric internal variability and external forcing (Zhang et al. 2022a). Low temperatures tend to appear in China when the East Asian winter monsoon is strong, and vice versa (Wang and Chen 2014b). The Siberia high and the East Asia trough are the two main factors responsible for the occurrence of extreme cold events in East Asia (Zuo et al. 2015). The increase in the Ural blocking could enhance cold advection from the polar region and trigger downstream cold air intrusions, which is favorable for the occurrence of extreme cold events in Hong Kong (Cheung et al. 2015). It has been indicated that the cold events during La Niña winters were contributed by the Ural blocking owing to the loss of Arctic sea ice in the Barents Sea, whereas those during El Niño winters were closely related to the negative Arctic Oscillation (AO, Chen et al. 2013; Song and Wu 2022). In addition, Wang et al. (2023) found that, on interannual time scales, the AO and El Niño–Southern Oscillation (ENSO) could significantly modulate the first and second modes of the winter extreme cold events in China before the 1980s, respectively. Reversed relationships of the two dominant modes with the AO and ENSO were observed after the 1980s (Wang et al. 2023).

A remarkable progress has been made in understanding the mechanisms responsible for the interannual variability of extreme cold events. Nevertheless, few studies have attempted to understand the quantitative contributions of atmosphere-surface coupled thermodynamic processes to extreme cold events. The coupled atmosphere-surface climate feedback-response analysis method (CFRAM) can directly isolate individual contributions of multiple physical and dynamical processes to surface temperature differences between two climate states (Cai and Lu 2009; Lu and Cai 2009; Zhang et al. 2022a). It has been proven to be an efficient offline diagnostic tool and successfully applied to quantify the relative contributions of various climate feedback processes to the surface and atmospheric temperature anomalies associated with ENSO (Deng et al. 2012; Park et al. 2012; Hu et al. 2016), the Northern Annular Mode (Deng et al. 2013), global warming (Chen et al. 2017, 2018; Hu et al. 2018, 2021; Kong et al. 2022), and the inter-model warming spread (Hu et al. 2020). The CFRAM has also been adapted to quantitatively examine the feedback attribution of surface temperature anomalies associated with the heatwaves over East Asia (Seo et al. 2021; Ha et al. 2022).

In addition to the dynamical processes, previous studies have found that the anthropogenic signal could be robustly detected in the changes in temperature extremes (Dong et al. 2018; Melbourne et al. 2019). In the CMIP5 multi-model warming projection, the anthropogenic greenhouse forcing and subsequent water vapor feedback processes are primarily responsible for the surface warming over East Asia (Fan et al. 2021). Recently, Zhang et al. (2022a) conducted a quantitative attribution analysis of the surface temperature anomalies associated with a record-breaking warm winter (2016/2017) in China by utilizing an updated version of CFRAM in which the effects of aerosols and more species of trace gases were incorporated (CFRAM-A hereafter). It was reported that the overall warming pattern of extreme warm winter in 2016/17 might be largely attributed to the effects of anomalous water vapor, atmospheric dynamics, and aerosols (Zhang et al. 2022a). Up to date, the relative roles of various physical processes associated with winter extreme cold events in China remain to be disclosed.

This study provides a quantitative attribution of individual physical and dynamical processes for the surface temperature anomalies associated with extreme cold events in China, utilizing the CFRAM-A. The rest of this paper is organized as follows. The datasets and method applied are described in Sect. 2. The quantitative attribution of individual physical and dynamical processes for the surface temperature anomalies in the extreme warm and cold winters are discussed in Sect. 3. Finally, conclusions of the study and further discussions are provided in Sect. 4.

2 Data and analysis methods

The quality-controlled observational station data of daily 2-m air temperature in 1964 meteorological stations across China during 1962–2019 is collected from the China National Stations' Fundamental Elements Datasets V3.0 (Cao et al. 2016; Ren et al. 2012). The method of calculating extreme cold events is the same as that of Wang et al. (2023), but for daily mean temperature. Specifically, an extreme cold day is identified when the daily mean temperature is below the 10th percentile of daily mean temperature during the period 1962–2019 (10th percentile for a total of 870 days; 58×15; the 15 days correspond to 7 days on either side of the target date). The number of extreme cold events is defined as the cumulative number of extreme cold days during each winter (Wang et al. 2023). The winter of a specific year is defined as the December of the preceding year and the January and February of the current year. The Empirical Orthogonal Function (EOF) analysis is applied to extract the dominant modes of extreme cold events in China (North et al. 1982; Dawson 2016; Wang et al. 2023).

Monthly mean geopotential height, winds, solar irradiance at the top of the atmosphere (TOA), ozone mixing ratio, air temperature, surface temperature, specific humidity, cloud amount, cloud liquid and ice water content, black carbon mixing ratio, organic carbon mixing ratio, sulfate aerosol mixing ratio, sea salt mixing ratio, dust mixing ratio, surface albedo, surface latent flux, and surface sensible heat

flux from the MERRA-2 reanalysis product are utilized (Gelaro et al. 2017). The MERRA-2 has a horizontal resolution of $0.5° \times 0.625°$ and 42 pressure levels ranging from 1000 to 0.1 hPa. Monthly trace gases mixing ratio (CO_2 and CH_4) are obtained from https://ads.atmosphere.copernicus.eu/cdsapp#!/dataset/cams-global-greenhouse-gas-inversion. The CO_2 concentration has a horizontal resolution of $1.9° \times 3.75°$ and 39 model levels from surface to TOA for 1979–2021. The CH_4 concentration has a horizontal resolution of $2° \times 3°$ and 34 model levels from surface to TOA for 1990–2020.

Daily mean geopotential height, winds, air temperatures, and vertical velocity from the fifth generation European Centre for Medium-range Weather Forecasts reanalysis (ERA5; accessed from the Copernicus Climate Change Service Climate Data Store) with a horizontal resolution of $1° \times 1°$ are applied to diagnose the thermal process by the following the thermodynamic energy equation (Hersbach et al. 2020):

$$\frac{\partial T}{\partial t} = \underbrace{-\boldsymbol{V} \cdot \nabla T}_{-advT} \underbrace{-\omega \frac{T}{\theta}\frac{\partial \theta}{\partial p}}_{-dTdp} + \underbrace{\frac{\dot{Q}}{C_p}}_{DH} , \quad (1)$$

where $-advT$ is the horizontal temperature advection, $-dTdp$ is the adiabatic heating due to vertical motion, and DH is the diabatic heating. Air temperature (T), the horizontal wind ($\boldsymbol{V}$), and omega (ω) are extracted from the ERA5 reanalysis datasets, whereas θ, the potential temperature, is derived from T using the Poisson's equation (Cheung et al. 2013). $\dot{Q}$ is the diabatic heating rate per unit mass (obtained from the thermodynamic energy equation), and C_p is the specific heat at constant pressure ($= 1004.07$ J K^{-1} kg^{-1}).

The CFRAM is based on the total energy balance in surface-atmosphere column, in order to isolate local partial temperature changes due to various individual radiative and dynamical processes (Cai and Lu 2009; Lu and Cai 2009). Following Zhang et al. (2022a), an updated version of the CFRAM that incorporates the effect of aerosols and more species of trace gases (namely the CFRAM-A) is applied in this study. The total temperature change can be decomposed as:

$$\Delta T = \left(\frac{\partial R}{\partial T}\right)^{-1} \left[\Delta S^{(SR)} + \Delta (S - R)^{(GHG)} + \Delta (S - R)^{(CLD)} \right.$$
$$+ \Delta S^{(AL)} + \Delta (S - R)^{(WV)} + \Delta (S - R)^{(O_3)}$$
$$\left. + \Delta (S - R)^{(AER)} + \Delta Q^{(atmos\_dyn)} + \Delta Q^{(surf\_dyn)+}\right], \quad (2)$$

where ΔT is the local total temperature difference between two climate states in each atmospheric layer and at the surface. $\left(\frac{\partial R}{\partial T}\right)^{-1}$ is the Planck feedback matrix, which obtains the change in the vertical structure of radiative warming or

cooling rate due to 1 K warming with respect to the base climate state in each layer. ΔS and ΔR are the changes in the convergence of shortwave radiation flux and the divergence of longwave radiation flux, respectively. SR, CLD, AL, WV, and O_3 represent solar irradiance, cloud, surface albedo, water vapor, and ozone, respectively. GHG refers to greenhouse gases, including methane (CH_4) and carbon dioxide (CO_2). AER stands for aerosols including black carbon, organic carbon, sulfate, sea salt, and dust. $\Delta Q^{(atmos\_dyn)}$ and $\Delta Q^{(surf\_dyn)}$ are the convergence of total non-radiative energy due to the changes in atmospheric dynamics and surface dynamics, estimated as a residual from the radiative energy perturbations. For more details, refer to Zhang et al. (2022a).

According to Wang et al. (2023), the dominant modes of the extreme cold events in China exhibited an interdecadal shift around the 1990s. In addition, more accurate datasets and a rather "clean" aerosol background without major volcanic eruptions could be obtained after 1996 (Zhang et al. 2022a). Therefore, we consider the averaged winter state of 1996–2019 as the base state, and the warm (cold) winter averaged state as the contrast to the base state.

3 Results

The in-situ observations of climatological extreme cold events and the first EOF mode of the cold days in boreal winter are presented in Fig. 1a–b for 1996–2019. The winter cold extremes occur around 4–8 days per year and are concentrated mostly over central-southwestern China (Fig. 1a). The first EOF mode of cold days shows a national-coherent distribution with a maximum of interannual variability over northern and central-southwestern China (Fig. 1b), similar to the climatological structure. These features are consistent with the result of Wang et al. (2023) for the period of 1993–2017. The time series of national-averaged cold days and the corresponding principal of the first EOF mode exhibit similar interannual variations (Fig. 1c), which are associated with the temperature anomalies in winter (Cheung et al. 2015; Wang et al. 2023). We define an extreme cold winter when the number of national-averaged cold days is above 0.8 standard deviations, and an extreme warm year when it is below − 0.8 standard deviations, in order to further investigate the temperature anomalies associated with winter extreme cold events. There are 5 extreme cold winters (2000/2005/2008/2011/2013) and 6 extreme warm winters (1999/2002/2004/2007/2015/2017) from 1996 to 2019 (Fig. 1c). The extreme cold winters exhibit nationwide negative surface temperature anomalies over China and the maximum anomaly center appears over northern and central-southwestern China (Fig. 2a). The extreme warm winters also present a national-coherent structure with maximum positive values over northern China (Fig. 2b). These
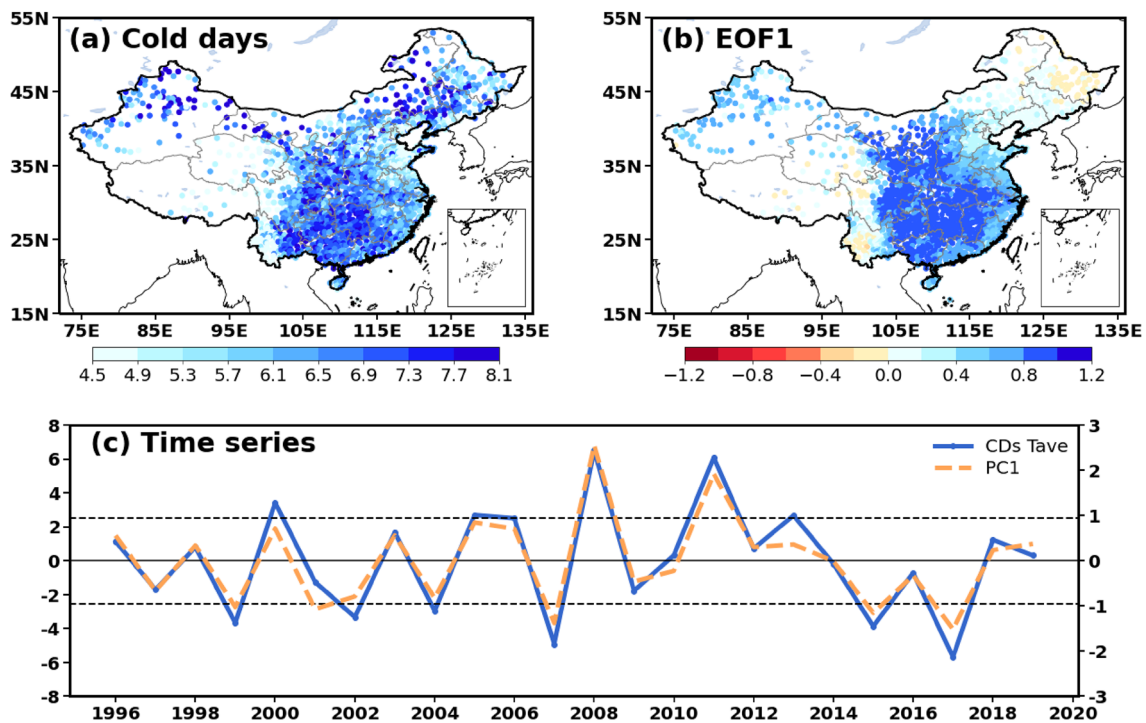
Fig. 1 **a** Climatological cold days and **b** the first EOF mode of cold days in boreal winter (DJF) during 1996–2019 from in-situ observations. **c** Detrended time series of China winter cold days (thick blue line) and the corresponding PC1 (dashed orange line). The dashed horizontal lines represent the 0.8 standardized deviations of the cold days

spatial patterns of surface temperature anomalies observed in the extreme cold and warm winters, including the magnitude and maximum centers, can be well captured by the MERRA-2 (Fig. 2). Thus, the MERRA-2 data is utilized for the CFRAM-A calculations to quantitatively attribute the surface temperature anomalies in the extreme warm and cold winters.

3.1 Quantitative attribution of surface temperature anomalies in extreme cold winters

The result from CFRAM-A calculations for extreme cold winters is shown in Fig. 3. The MERRA-2 surface temperature differences and the sum of partial surface temperature differences between the cold winters and the 1996–2019 base state derived from the CFRAM-A analysis are presented in Fig. 3a, b. Apparently, the CFRAM-A calculations well reproduce the spatial structure and the magnitude of surface temperature anomalies in the MERRA-2 (Fig. 3a, b). The area-averaged sum of partial surface temperature differences over China is about −0.85 K from the CFRAM-A calculations, which is quite close to the number of −0.86 K in the MERRA-2 (Fig. 3a, b). The errors associated with the offline calculation and linearization process are quite small at the surface (figure not shown), as validated by previous studies (Chen et al. 2017; Park et al. 2012). Therefore, the

CFRAM-A is reliable by using the time-mean atmospheric and surface fields in the offline radiative transfer calculations and the linearization of radiative energy perturbations (Seo et al. 2021; Zhang et al. 2022a).

The quantitative contribution of individual physical and dynamical processes to the surface temperature anomalies in extreme cold winters is presented in Fig. 3c–l. The processes associated with surface albedo contribute to an overall cooling of −0.46 K in China, the effect that shows a similar structure to the total temperature differences (Fig. 3g). The anomalies of water vapor provide almost a uniform cooling effect, which induce −0.26 K overall cooling (Fig. 3h). In addition, the processes associated with atmospheric dynamics and aerosols exhibit area-averaged partial surface temperature differences of −0.11 K and −0.07 K, respectively (Fig. 3j, l). Specifically, the processes associated with aerosols provide a considerable cooling effect over central-eastern China but a warming effect in the southwestern region (Fig. 3i). The atmospheric dynamics contribute to cooling effects over most parts and warming over northeastern China (Fig. 3l). Although the effect of cloud is negligible for the national-averaged temperature differences, it provides a considerable cooling over southern China (Fig. 3i). The effect of surface dynamics is the only negative contributor, which shows a remarkable warming in eastern China and a relatively weaker cooling in western China (Fig. 3k). It
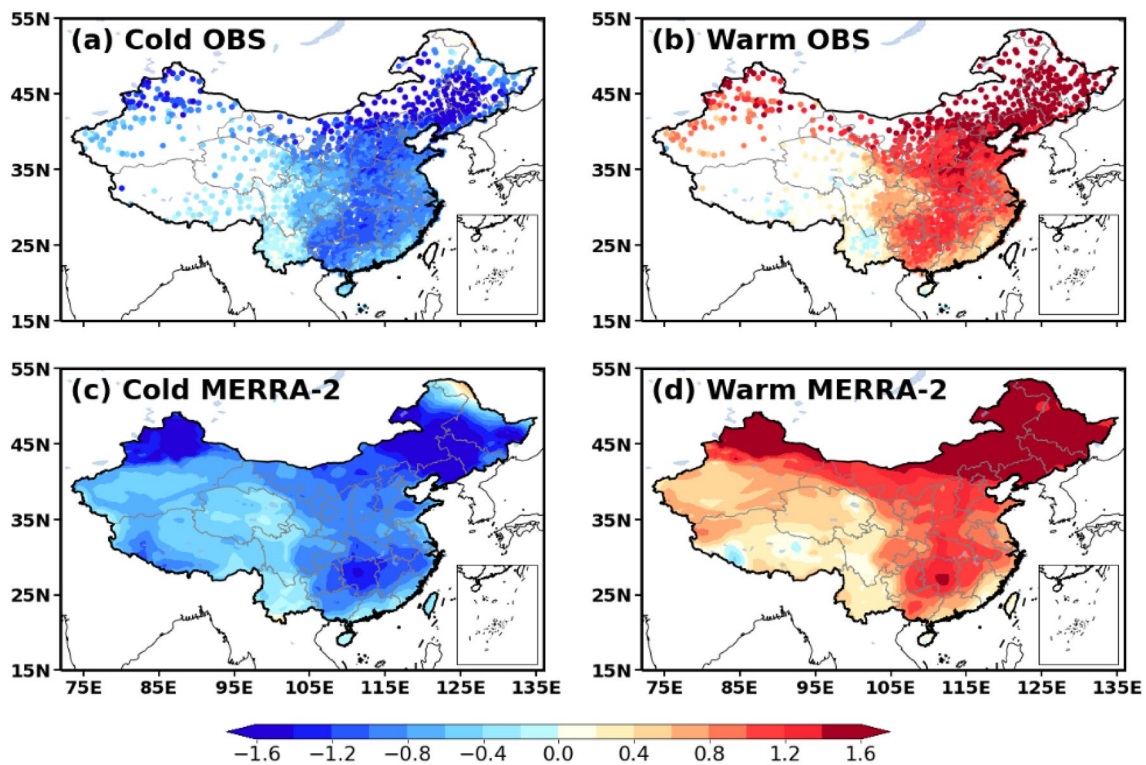
Fig. 2 Surface temperature anomalies (°C) with respect to the 1996–2019 climatology in extreme cold winters from **a** in-situ observations and **c** MERRA-2. **b**, **d** Same as in (**a**, **c**), but for extreme warm winters

provides an overall warming of 0.09 K for the extreme cold winters. On the other hand, the changes in solar irradiance, ozone, CO_2, and CH_4 exert a negligible impact on the surface temperature difference in extreme warm winters (Fig. 3c–f). Overall, the remarkable cooling in northeastern China is primarily attributed to the changes in albedo and water vapor, whereas the changes in albedo, water vapor, atmospheric dynamics, and aerosols jointly contribute to the cooling in central-southern China.

We further calculate the spatial 'pattern-amplitude' (PAP) coefficient, following Park et al. (2012) and Deng et al. (2013), to quantify the overall contributions of individual processes to surface temperature changes. The PAP coefficient is defined as:

$$PAP_i = \langle \Delta T \rangle \times \frac{\langle \Delta T_i \Delta T \rangle}{\langle (\Delta T)^2 \rangle}, \tag{3}$$

where ΔT is the total surface temperature anomalies with respect to the winter base state of 1996–2019. PAP_i and ΔT_i are the spatial PAP coefficient and partial surface temperature anomalies related to the ith process. and $\langle \rangle$ denotes the calculation of area average. The sum of all PAP_i equals to the area average of the total surface temperature anomalies.

Figure 4a presents the PAP coefficients associated with the ten partial temperature differences shown in Fig. 3c–l, and their sums over China. Consistent with the above analysis, albedo and water vapor act as the main positive contributors to the cooling in China for the cold cases, and atmospheric dynamics and aerosols play a secondary positive role (Fig. 4a). Those positive effects are compensated by the negative contribution of surface dynamics to some extent (Fig. 4a). The relative roles of the physical processes vary in different regions. Specifically, the cooling in northeastern China is mainly attributed to the processes associated with albedo, whereas the effects of atmospheric dynamics play the dominant roles in central-eastern China cooling (Fig. 4c, d). The processes of atmospheric dynamics play an opposite role in northeastern China compared to other regions (Fig. 4b–d), resulting in a weaker overall effect of atmospheric dynamics for the national-averaged cooling.

We further investigate the anomalies of 925-hPa geopotential height and winds, precipitable water, snow cover, and aerosol optical depth (AOD) to explore the possible causes of partial temperature changes in the extreme cold winters (Fig. 5). At the lower troposphere, anomalous negative geopotential height appears over the high latitudes, but anomalous positive geopotential height dominates
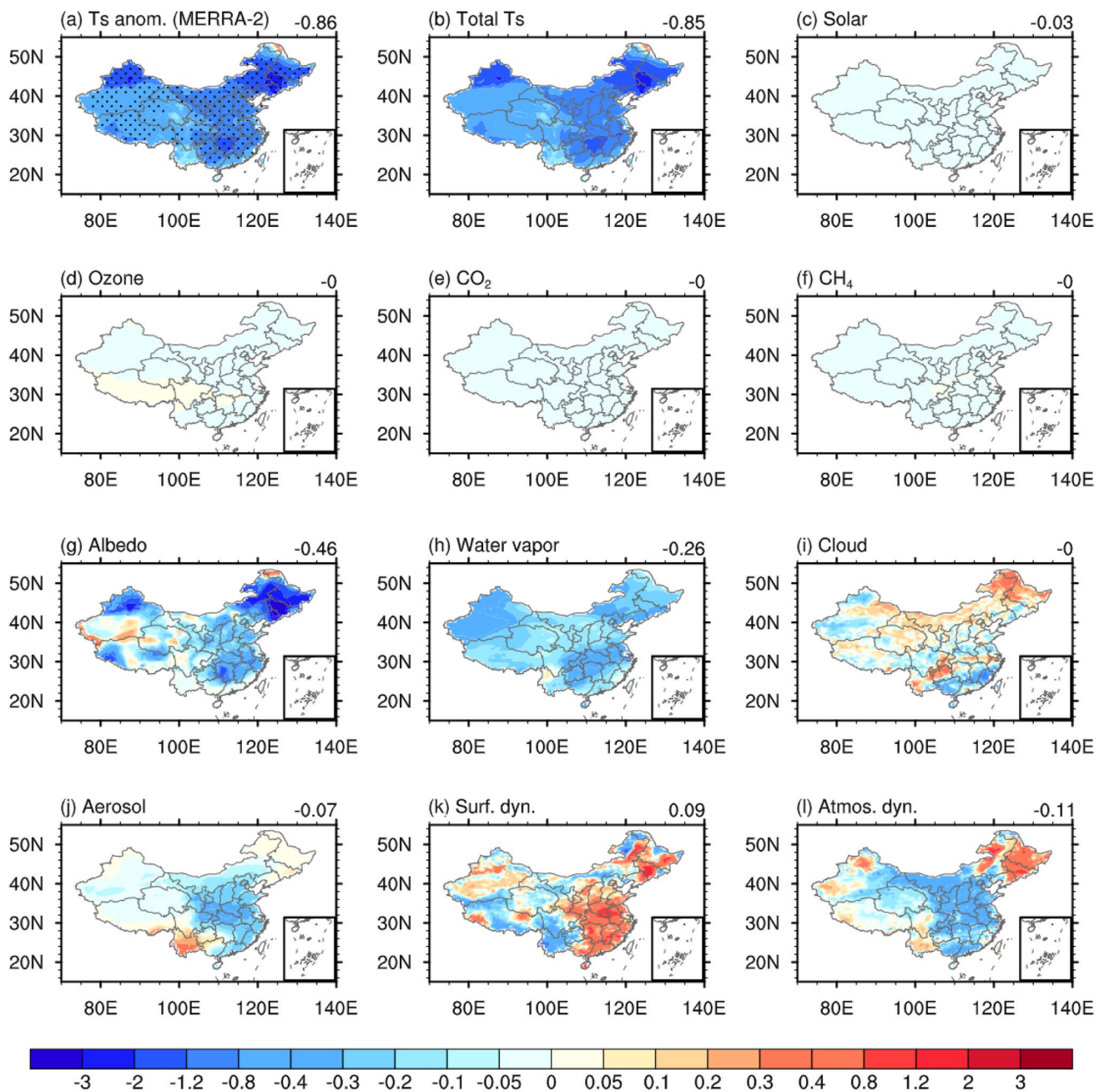
Fig. 3 **a** Surface temperature differences (K) in winters between cold cases and 1996–2019 base state in MERRA-2. **b** Sum of partial surface temperature differences (K) derived from the CFRAM-A, and partial surface temperature differences (K) due to the changes in **c** solar irradiance, **d** ozone, **e** CO_2, **f** CH_4, **g** surface albedo, **h** water vapor, **i** clouds, **j** aerosols, **k** surface dynamics, and **l** atmospheric dynamics. Stippling in **a** denotes the values exceeding the 0.5 standard deviations of 1996–2019 inter-annual variation. The number on the upper right of each panel denotes the area-averaged value over China

over the mid-latitudes (Fig. 5a). The geopotential height shows positive and negative anomalies at lower levels over northern and southern East Asia, respectively, enhancing the north–south pressure gradient (Fig. 5a). An anomalous negative geopotential height and a cyclonic circulation anomaly appear at the mid-upper levels over the mid-latitudes of East Asia (figure not shown). These features are similar to those for the negative phase of the AO, which favor the development of the East Asian trough, leading to cold advection from the high latitudes (Fig. 5a, b). On the other hand, the quasi-barotropic positive geopotential height anomalies over northeastern China contribute to the local warming effect (Figs. 3l and 5a).

The spatial pattern of snow cover anomalies is similar to the contribution of surface albedo for surface temperature changes (Figs. 3g and 5d). The local snow cover anomalies are dominant in the change of surface albedo. Specifically, the positive anomalies of snow cover increase the surface albedo, reflecting more incident solar radiation and leading to cooling over China, in particular for northeastern China and north of Xinjiang Uygur Autonomous Region (Figs. 3b, g and 5d). This result demonstrates that the contribution of surface albedo to surface temperature changes is primarily related to the change in local snow cover. Water vapor act as a greenhouse gas, and more water vapor provides a warming effect and vice versa. The cooling effect of water vapor is clearly linked to the below-normal precipitable water (Figs. 3h and 5c).

Moreover, the effect of aerosols is related to the AOD change in the extreme cold winters (Fig. 6a–f). By scattering or absorption of incoming shortwave solar radiation, an increase (a decrease) in aerosol concentration basically contributes to cooling (warming) in surface temperature. The cooling and warming effects of aerosols are associated with the positive anomalies of AOD over most of China and the negative anomalies of AOD over the southwestern edge of China, respectively (Figs. 3j, 5e and 6a). In fact, the cooling effect of aerosols in central China is mainly due to the change in sulfate, whereas the warming effect in southwestern China is linked to the changes in organic carbon (Fig. 6a–e). In northwestern China, the cooling effect of aerosols is dominated by the change in dust (Fig. 6a, f).

The total cloud cover presents positive anomalies over most parts of China and negative anomalies in most of south China and Xinjiang Uygur Autonomous Region in the extreme cold winters (Fig. 7a), which seems to be inconsistent with the surface temperature differences induced by clouds (Fig. 3i). We further decompose the total temperature changes related to clouds into partial temperature changes associated with the long-wave and short-wave effects of clouds (Fig. 7b, c). In general, an increase in total cloud cover causes less incident solar radiation to reach the surface (i.e., short-wave effect), resulting in surface cooling and vice versa (Fig. 7a, 7c). In addition, more clouds add downward long-wave radiation, exerting a warming effect on surface temperature changes (Fig. 7a, b). Although total cloud cover shows only a slightly positive anomaly over southern China (except for the Guangdong Province), the short-wave related cloud effect contributes to a remarkable surface cooling (Fig. 7a, c). On the other hand, the long-wave related cloud effect is stronger than the short-wave related cloud effect in northern China (Figs. 7c–d and 3i). The cloud effects are dominated by its short-wave radiation effect in south China and long-wave radiation effect in the rest of China.

3.2 Quantitative attribution of surface temperature anomalies in extreme warm winters

For the warm cases, the partial surface temperature differences derived from the CFRAM-A are presented in Fig. 8c–l. In the extreme warm winters, the area-averaged surface temperature difference over China is approximately 0.91 K, and that derived from the CFRAM-A calculations is 0.89 K (Fig. 8a, b). The spatial structure and magnitude of the surface temperature anomalies in the MERRA-2 are also well reproduced by the CFRAM-A calculations (Fig. 8a, b). Similar to the cold cases, the feedback processes in solar irradiance, ozone, CO_2, and CH_4 exert negligible impacts on the surface temperature anomalies in the extreme warm winters (Fig. 8c–f). The atmospheric dynamics inducing 0.43 K area-averaged warmings play a major role in the temperature anomalies over most parts of China for the extreme warm winters (Fig. 8l). The processes associated with water vapor, surface albedo, and aerosols also make considerable contributions (0.17 K, 0.13 K, and 0.07 K area-averaged warming, respectively; Fig. 8g–j). Specifically, the process associated with water vapor exerts a considerable warming effect over most of China but a cooling effect over southeastern China (Fig. 8h). Surface albedo exhibits a cooling effect in northernmost China and almost a warming effect in the rest of China (Fig. 8g). The spatial pattern of the aerosol effect is depicted by a dipole structure, with cooling in southern China and warming in central China (Fig. 8j). The effects of cloud and surface dynamics present large regional features and make only moderate contributions to the overall warming (0.02 K and 0.01 K, respectively; Fig. 8i, k), consistent with Zhang et al. (2022a). In particular, the cloud effect is characterized by a remarkable warming in southern China (Fig. 8i).

Overall, atmospheric dynamics act as a main positive contributor to the nation-wide warming in China for extreme warm winters, and the processes associated with albedo and water vapor play a secondary role (Fig. 4e). Specifically, the warming in northeastern China is mainly attributed to the processes associated with atmospheric dynamics, water vapor, and albedo, whereas the effects of atmospheric dynamics, aerosols, and albedo play the dominant roles in central-eastern China warming (Fig. 4f, g). In southern China, the warming is primarily attributed to the changes in clouds, compensated by the cooling effects of water vapor and aerosols (Fig. 4h).

The anomalies of 925-hPa geopotential height, winds, precipitable water, snow cover, and AOD in the extreme warm winters are presented in Fig. 9. At the lower troposphere, anomalous negative geopotential height appears over the high latitudes, but anomalous positive geopotential height dominates over the mid-latitudes (Fig. 9a). The
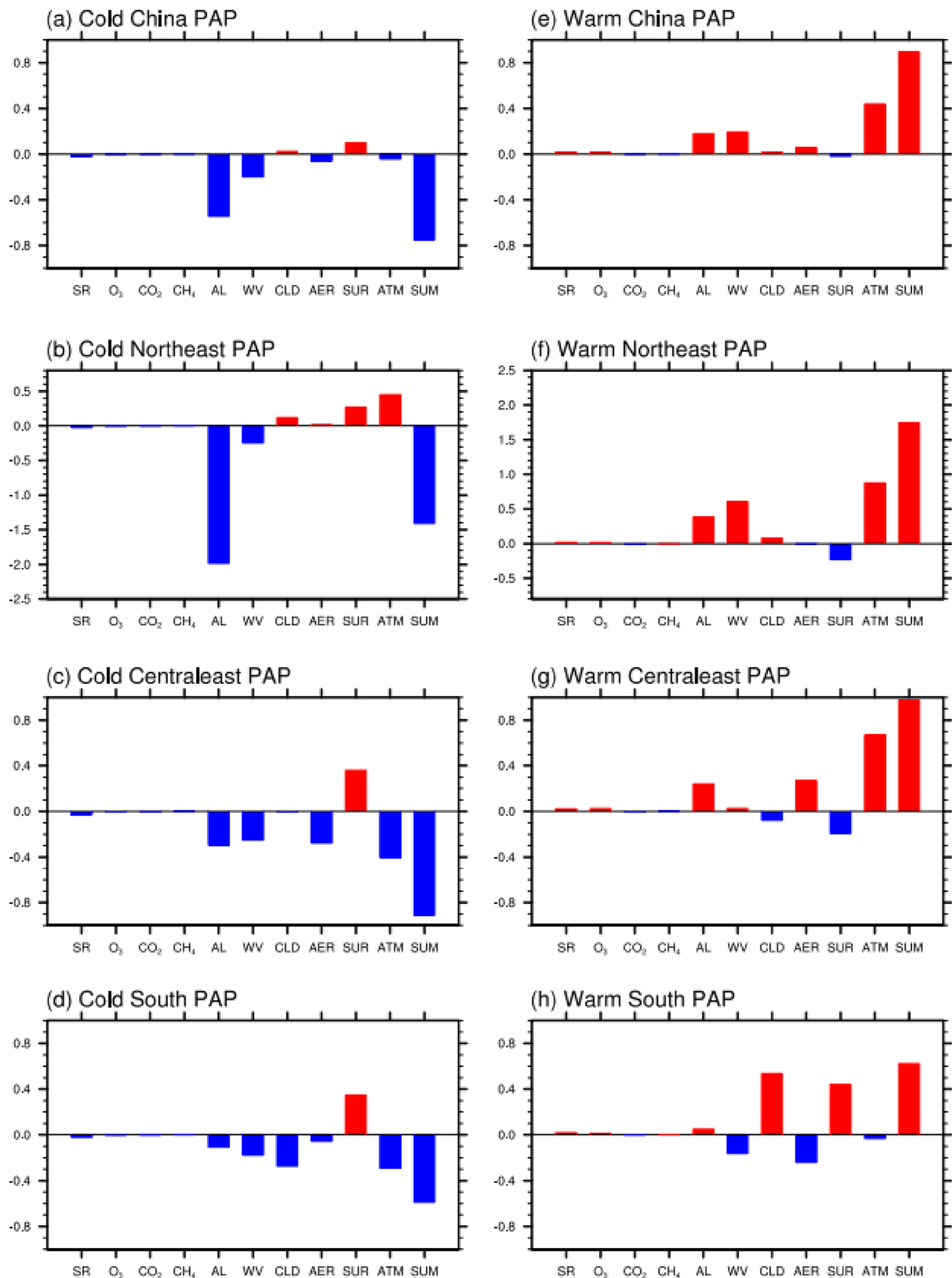
◄**Fig. 4** The PAP coefficients (K) associated with the partial temperature differences and their sums over **a** China, **b** northeastern China, **c** central-eastern China (30°–40° N, 105°–120 °E) and **d** southern China (20°–25° N, 105°–120 °E) for extreme cold winters. **e–h** Same as in (**a–d**), but for extreme warm winters. The abbreviation 'SR', 'O$_3$', 'CO$_2$', 'CH$_4$', 'AL', 'WV', 'CLD', 'AER', 'SUR', 'ATM', and 'SUM' stand for the processes of solar irradiance, ozone, carbon dioxide, methane, surface albedo, water vapor, cloud, aerosols, surface dynamics, atmospheric dynamics, and the sum, respectively

upper and middle troposphere displays a similar structure of geopotential height anomalies (figure not shown). Anomalous positive geopotential height and anticyclonic circulations occupy major parts of China. These features signify a positive phase of the AO. According to Wang et al. (2023), these circulation anomalies associated with the positive AO are unfavorable for deepening the East Asian trough, and hence result in anomalous warm temperature advection and adiabatic heating over most of China (Fig. 9b), contributing to the warming effect of atmospheric dynamics in the extreme warm winters (Fig. 8l).

In the extreme warm winters, below-normal snow cover appears over most of China, leading to reduce in the surface albedo which reflects fewer incident solar radiation and induces surface warming over China (Figs. 8b, g and 9d). The positive anomalies of snow cover increase the surface albedo, reflecting more incident solar radiation and leading to cooling over the northernmost of China (Figs. 8g and 9d). The warming (cooling) effect of water vapor over major parts (southeast) of China is clearly linked to above-normal (below-normal) precipitable water (Figs.. 8h and 9c). The cooling and warming effects of aerosols are associated with the negative anomalies of AOD over most of China and the positive anomalies of AOD over the southwestern edge of China, respectively (Figs. 8j and 9e). In fact, the warming effect of aerosols in central China is mainly due to the change in sulfate, whereas the cooling effect in southern China is linked to the changes in black carbon, organic carbon, and sea salt (Fig. 6g–k). In northwestern China, the warming effect of aerosols is dominated by the change in dust (Fig. 6g, l).

The total cloud cover presents negative anomalies over most of China and slightly positive anomalies over the northernmost parts in the extreme warm winters (Fig. 7d). Corresponding to the remarkable reduction of total cloud cover in southern China, the short-wave related cloud effect contributes to a maximum warming center whereas the long-wave related cloud effect shows a relatively weaker cooling in southern China (Fig. 7e–f). The cloud effects are dominated by its short-wave radiation effect in southern China and long-wave radiation effect in the rest of China, consistent with the cloud effects in the extreme cold winters.

3.3 Year-to-year variations among extreme warm and cold winters

The PAP coefficients associated with the partial surface temperature differences due to the changes in different processes in each warm and cold cases are shown in Fig. 10a for verifying whether the conclusions drawn from the composite analysis are applied to the individual cases. The processes associated with surface albedo and water vapor provide large positive contributions (cooling effects in the cold cases and vice versa) to the surface temperature changes for both extreme warm and cold years, and the effect of anomalous surface dynamics is a major negative contributor (Fig. 10a). The contributions provided by these three drivers are basically proportional to the total temperature anomalies. On the other hand, the influences of atmospheric dynamics display a larger year-to-year variation in the extreme cold years than in the extreme warm years, exhibiting asymmetric contributions to the warm and cold cases (Fig. 10a). Specifically, the atmospheric dynamics induce considerable warmings for the warm cases except in 2015. They show a dominant warming effect for 2017. On the other hand, for the extreme cold years, considerable effects of the atmospheric dynamics for overall cooling only appeared in 2005 and 2008 (Fig. 10a). This seemingly smaller overall effect is possibly because there exist opposite contributions of the atmospheric dynamics between northeastern China and other places (Fig. 3l). This spatially heterogeneous feature for the contribution of atmospheric dynamics to surface temperature change can also be seen from the individual extreme cold years (e.g., Fig. 11).

Aerosols provided considerable warming effects in the winters of 1999, 2000, 2002, and 2017, and cooling effects in the winters of 2008 and 2011 (Fig. 10a). It seems that the effect of aerosols does not entirely depend on the warm and cold cases. Instead, the contribution follows the changes in AOD which show negative anomalies before 2004 and after 2015 but positive anomalies in between (Fig. 10b). Given the dominant role of anthropogenic aerosols in the total aerosol effect as discussed in the previous sections, the case-by-case effect of aerosols is possibly related to industrialization development and the emission reduction policies in China since 2013 (Zhang et al. 2022a).

4 Summary and discussion

A quantitative attribution analysis of the surface temperature anomalies associated with winter extreme cold events in China is conducted in this study. The temperature anomalies exhibit almost a coherent spatial pattern, warming in extreme warm winters and cooling in extreme cold winters,
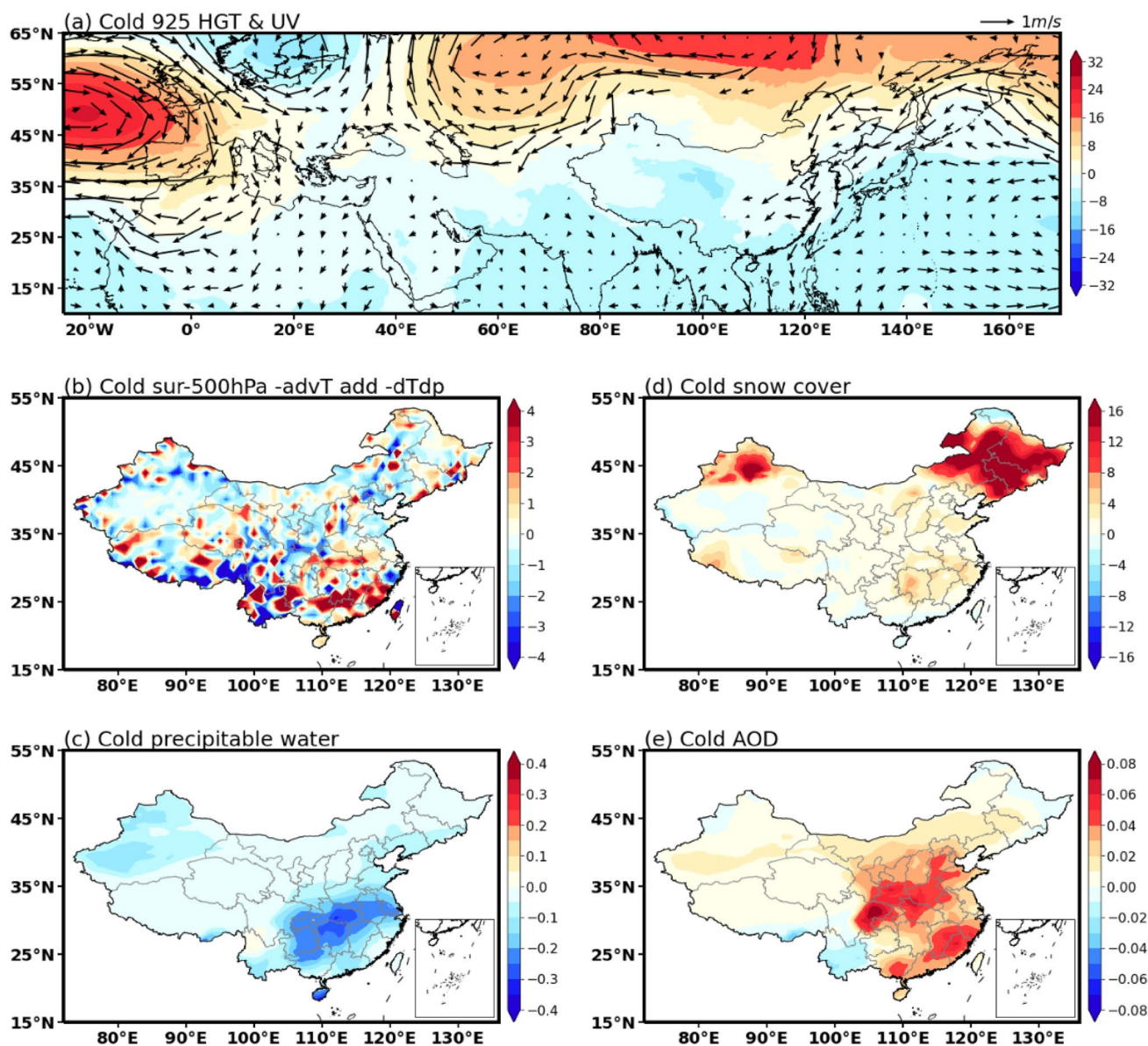
Fig. 5 Anomalies (with respect to the 1996–2019 base state) of **a** 925-hPa geopotential height (shading; hPa) and winds (vectors; m s^{-1}), **b** combined effect of the horizontal advection and adiabatic heating (vertically integrated from the surface to 500 hPa; K day^{-1}), **c** precipitable water (kg m^{-2}), **d** snow cover (%), and **e** AOD at 550 nm in extreme cold winters

with the maximum anomaly center over northern China. Using the CFRAM-A analysis method, we decompose the surface temperature anomalies into partial surface temperature changes due to the processes of solar irradiance, ozone, carbon dioxide (CO_2), methane (CH_4), surface albedo, water vapor, clouds, aerosols, surface dynamics, and atmospheric dynamics.

The effects of anomalous surface albedo, water vapor, atmospheric dynamics, and aerosols are the major positive contributors, and the processes associated with surface dynamics provide a major negative effect for both extreme warm and cold years. Specifically, the effect of surface albedo is directly linked to the change in local snow cover over China, which contributes to overall warming and cooling patterns for the extreme warm and cold years, respectively. The effect of water vapor is basically linked to precipitable water anomalies. The effect of aerosols may directly depend on the abnormal winter AOD, and considerable impacts of anthropogenic aerosols are detected over central-southern China, related possibly to industrialization development and the emission reduction policies in China since 2013. In addition, the cloud effect presents a
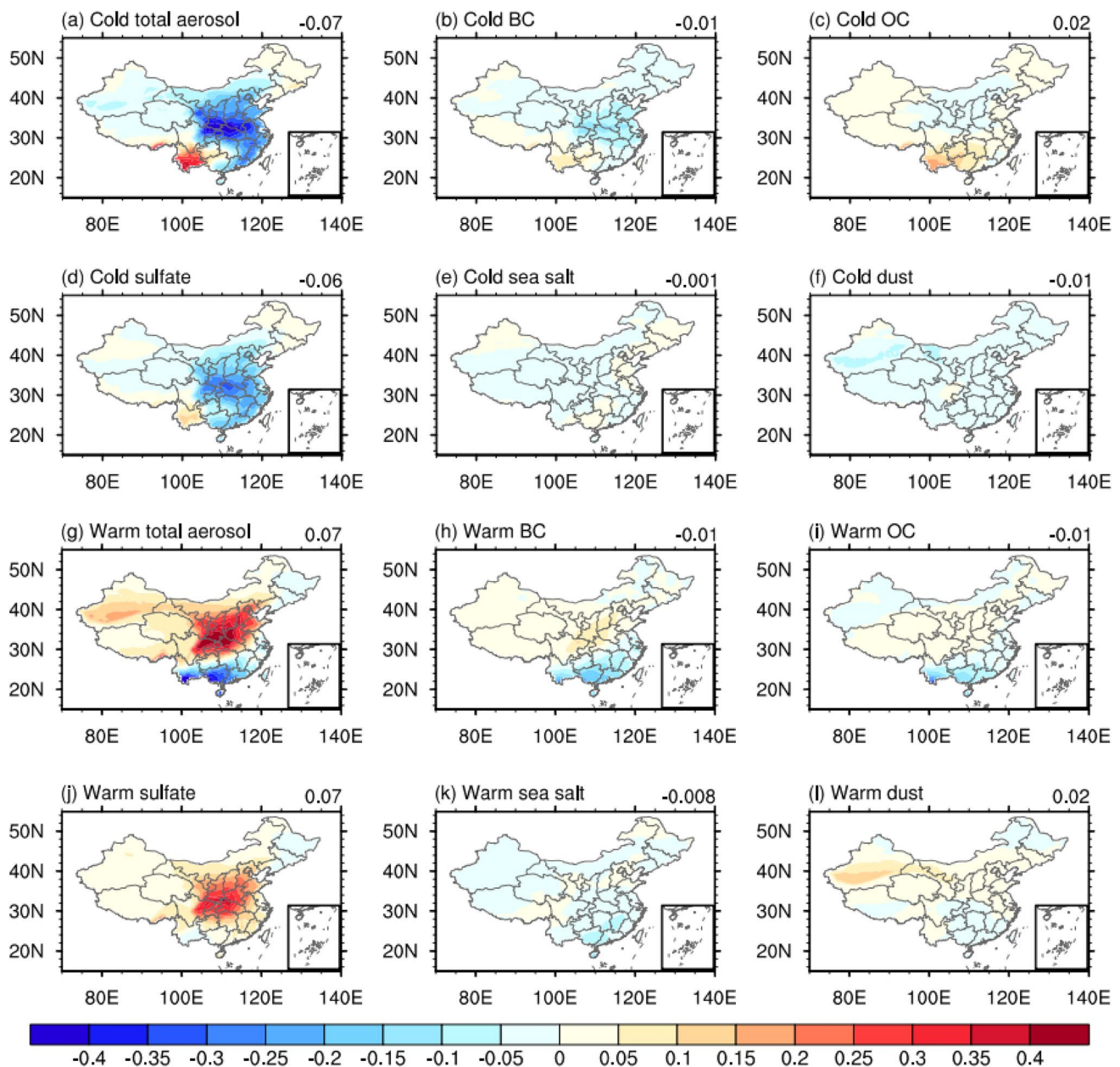
Fig. 6 Partial surface temperature differences (K) due to the changes in the **a** total aerosols, **b** black carbon, **c** organic carbon, **d** sulfate, **e** sea salt, and **f** dust in the cold winters. **g–l** Same as in (**a–f**), but for the warm winters. The number on the upper right of each panel denotes the area-averaged value over China

large regional dependent feature, which is dominated by its short-wave radiation effect in southern China and long-wave radiation effect in the rest of China. The decrease in total cloud cover in the extreme warm winters leads to remarkable warming in southern China, and vice versa for the extreme cold winters.

The processes associated with atmospheric dynamics exhibit asymmetric contributions between the extreme warm and cold years. They provide a coherent and dominant warming effect over most of China in the warm cases, which is likely associated with nation-wide warm air advection. On the other hand, the effects of atmospheric dynamics display large regional and year-to-year variations for the cold cases. The contribution of atmospheric dynamics to the surface temperature anomalies is out of phase in northeastern China compared to the other places. According to Wang et al. (2023), the effect of AO on extreme cold events is limited over northeastern China after the 1990s whereas
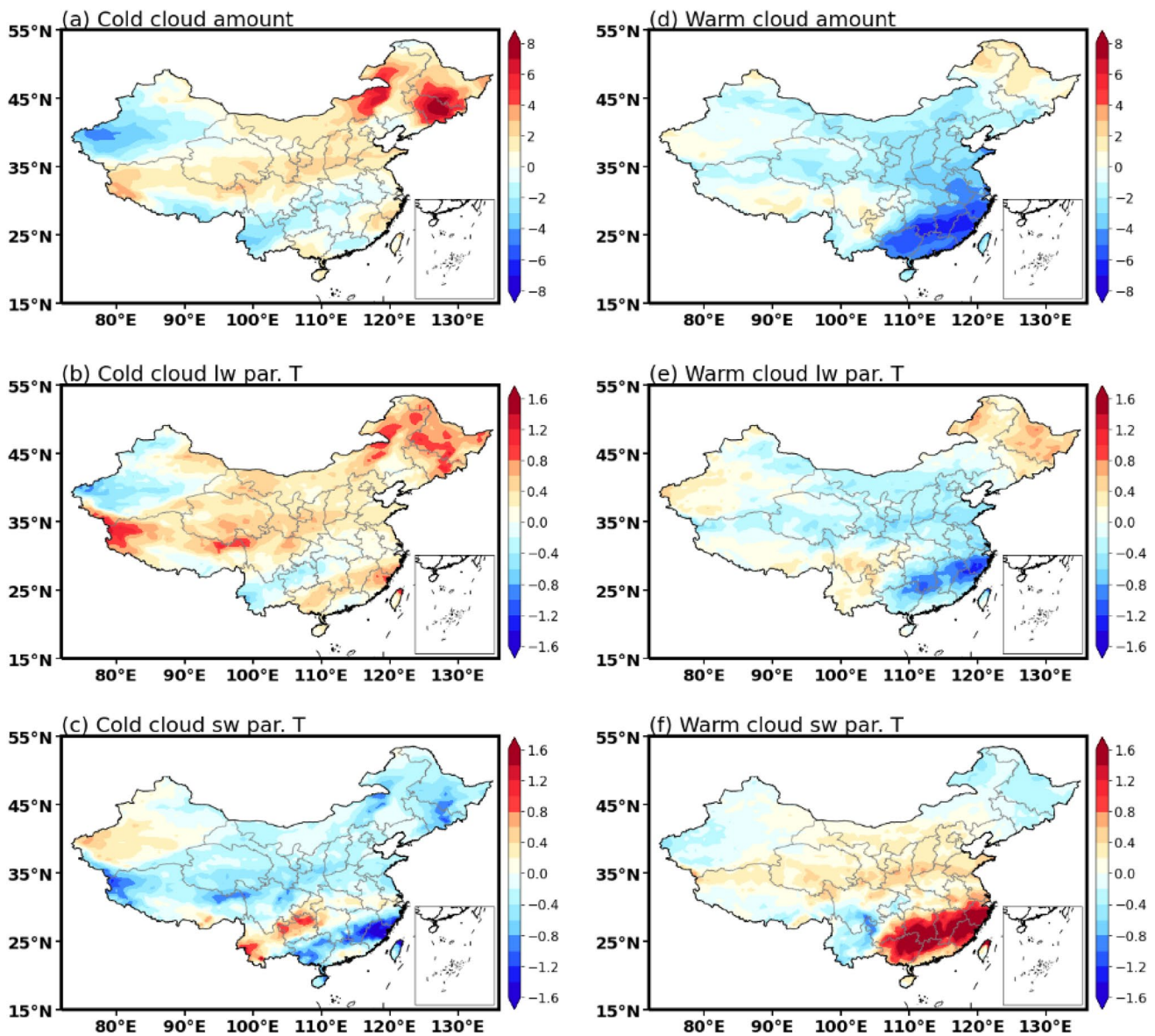
Fig. 7 Anomalies of **a** total cloud cover (%) in extreme cold winters, and partial surface temperature differences with respect to the 1996–2019 base state (K) due to the changes in **b** long-wave and **c** short-wave effects of clouds. **d–f** Same as in (**a–c**), but for extreme warm winters

ENSO could modulate the extreme cold events over southern China. Whether and to what extent the AO and ENSO contribute to the asymmetric contributions of atmospheric dynamics warrant further investigations.

The effects of greenhouse gases (e.g., CO_2 and CH_4) on interannual timescale are negligible in this work; however, they have been clearly detected as the dominant anthropogenic external forcings on the changes in extreme temperature under global warming or on the long-term scale (e.g., Dong et al. 2018). Numerous previous studies

have been focused on the anthropogenic greenhouse forcing in the future climate projections (Fischer and Knutti 2015; Bador et al. 2016; Alexander and Arblaster 2017; Lewis and King 2017; Di Luca et al. 2020; Fan et al. 2021; van der Wiel and Bintanja 2021). Fan et al. (2021) suggested that the anthropogenic greenhouse forcing and subsequent water vapor feedback processes were primarily responsible for the surface warming over East Asia. In addition, a considerable effect of warming associated with aerosols over southeastern China had been
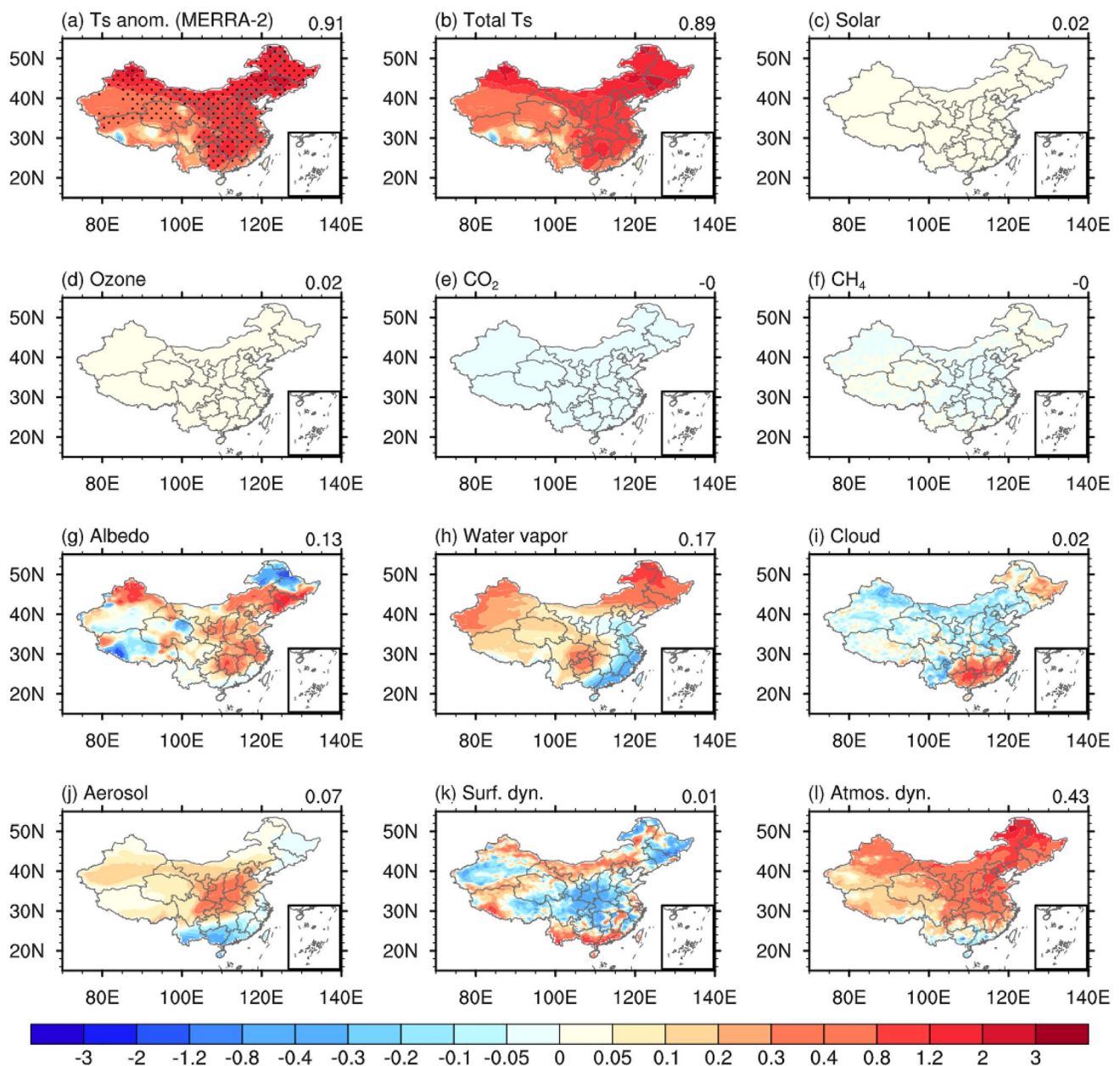
Fig. 8 Same as in Fig. 3, but for extreme warm winters

revealed by the CFRAM-A analysis in 2016/17 winter, and it may ultimately be attributed to the effectiveness of emission reduction policies implemented in China since 2013 (Zhang et al. 2022a). The warming effects due to the substantial decrease in aerosol concentration in China may be anticipated. Nevertheless, how the policies of mitigating pollution and reducing anthropogenic aerosols contribute to the surface temperature changes associated

with extreme cold events warrants further investigations. Recently, the Aerosol Chemistry Model Intercomparison Project has been endorsed by the Coupled-Model Intercomparison Project 6 and designed to quantify the climate impacts of aerosols (Collins et al. 2017). This provides an opportunity for our next work to investigate the regional climate impacts of future aerosol emission reduction policies in extreme temperature events.
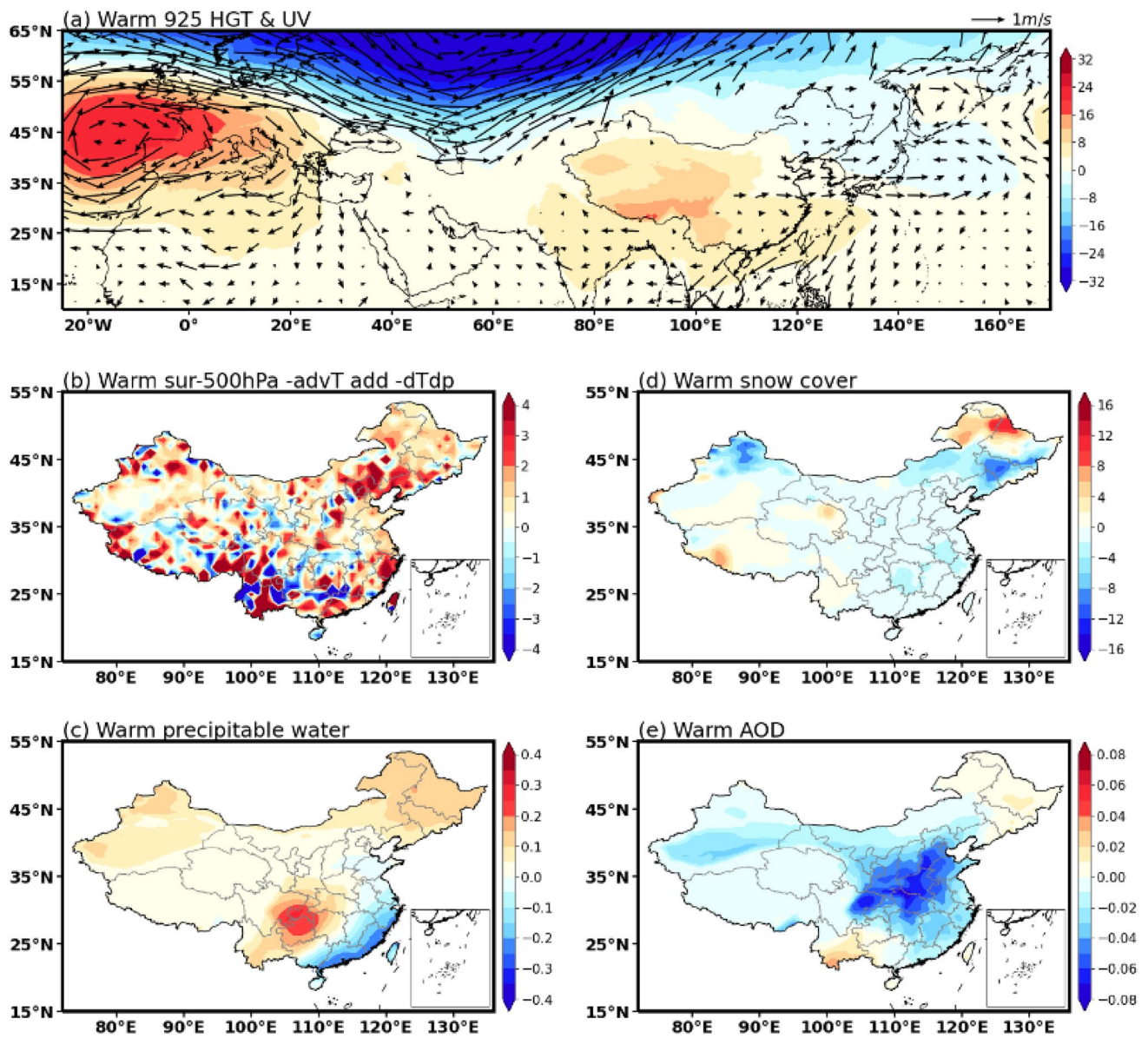
Fig. 9 Same as in Fig. 5, but for extreme warm winters

Fig. 10 a The PAP coefficients (K) as a function of extreme cold (light blue background) and warm (light red background) years associated with the partial surface temperature differences (K) due to the changes in solar irradiance, ozone, CO_2, CH_4, surface albedo, water vapor, clouds, aerosols, surface dynamics, and atmospheric dynamics. Different feedback processes are represented by different colors using the color scheme on the bottom. Abbreviations 'SR', 'O$_3$', 'CO$_2$', 'CH$_4$', 'AL', 'WV', 'CLD', 'AER', 'SUR', 'ATM', and 'SUM' stand for the processes of solar irradiance, ozone, carbon dioxide, methane, surface albedo, water vapor, cloud, aerosols, surface dynamics, atmospheric dynamics, and the sum, respectively. **b** Anomalies of winter AOD at 550 nm from 1996 to 2019. Blue (red) dots indicate extreme cold (warm) winters
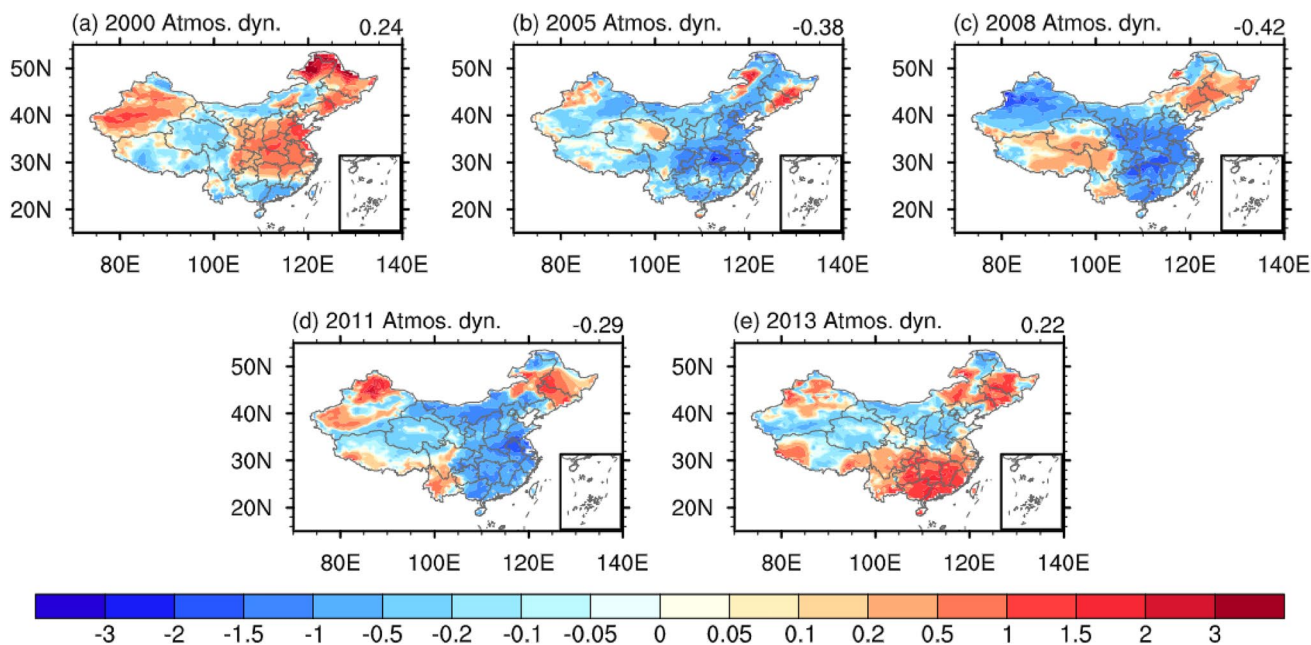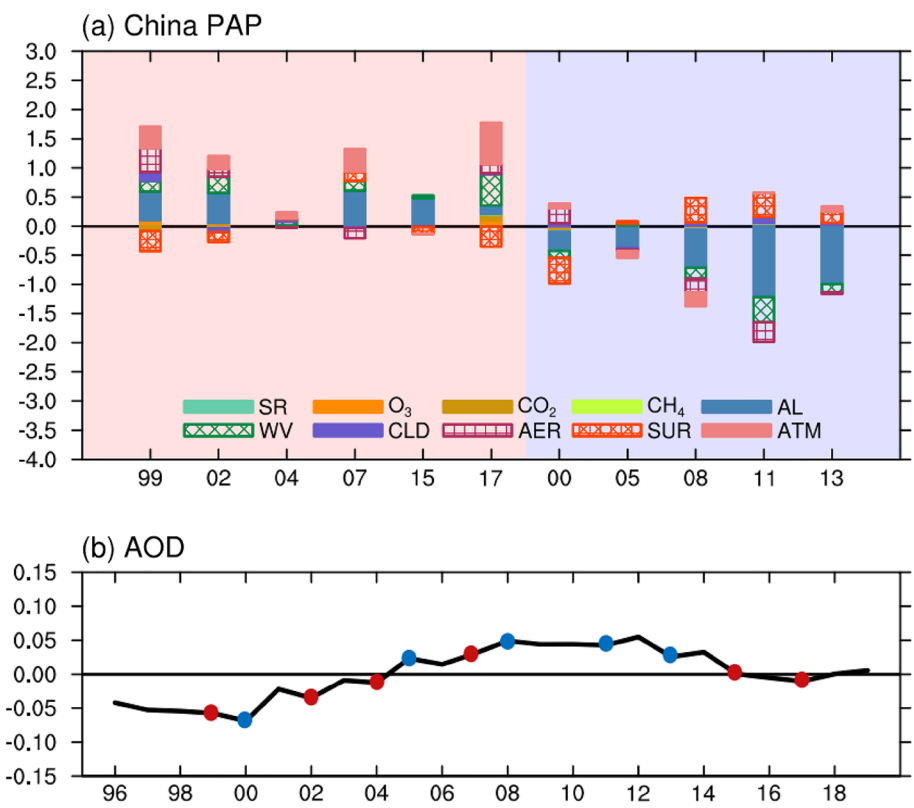
Fig. 11 Partial surface temperature differences (K) due to the changes in the atmospheric dynamics in winters of **a** 2000, **b** 2005, **c** 2008, **d** 2011, and **e** 2013. The number on the upper right of each panel denotes the area-averaged value over China

Declarations

References

Alexander LV, Arblaster JM (2017) Historical and projected trends in temperature and precipitation extremes in Australia in observations and CMIP5. Weather Clim Extrem 15:34–56. https://doi.org/10.1016/J.WACE.2017.02.001

Bador M, Terray L, Boé J (2016) Detection of anthropogenic influence on the evolution of record-breaking temperatures over Europe. Clim Dyn 46:2717–2735. https://doi.org/10.1007/S00382-015-2725-8/FIGURES/11

Cai M, Lu J (2009) A new framework for isolating individual feedback processes in coupled general circulation climate models. Part II: method demonstrations and comparisons. Clim Dyn 32:887–900. https://doi.org/10.1007/S00382-008-0424-4/TABLES/5

Cao L, Zhu Y, Tang G, Yuan F, Yan Z (2016) Climatic warming in China according to a homogenized data set from 2419 stations. Int J Climatol 36:4384–4392. https://doi.org/10.1002/joc.4639

Chen W, Lan X, Wang L, Ma Y (2013) The combined effects of the ENSO and the Arctic Oscillation on the winter climate anomalies in East Asia. Chin Sci Bull 58:1355–1362. https://doi.org/10.1007/S11434-012-5654-5

Chen J, Deng Y, Lin W, Yang S (2017) A process-based assessment of decadal-scale surface temperature evolutions in the NCAR CCSM4's 25-year hindcast experiments. J Clim 30:6723–6736. https://doi.org/10.1175/JCLI-D-16-0869.1

Chen J, Deng Y, Lin W, Yang S (2018) A process-based decomposition of decadal-scale surface temperature evolutions over East Asia. Clim Dyn 51:4371–4383. https://doi.org/10.1007/s00382-017-3872-x

Chen W, Wang L, Feng J, Wen Z, Ma T, Yang X, Wang C (2019) Recent progress in studies of the variabilities and mechanisms of the East Asian Monsoon in a Changing Climate. Adv Atmos Sci 36:887–901. https://doi.org/10.1007/s00376-019-8230-y

Chen W, Zhang R, Wu R, Wen Z, Zhou L, Wang L, Hu P, Ma T, Piao J, Song L, Wang Z, Li J, Gong H (2023) Recent advances in understanding multi-scale climate variability of the Asian Monsoon. Adv Atmos Sci. https://doi.org/10.1007/s00376-023-2266-8

Cheung HN, Zhou W, Shao Y, Chen W, Mok HY, Wu MC (2013) Observational climatology and characteristics of wintertime atmospheric blocking over Ural-Siberia. Clim Dyn 41:63–79. https://doi.org/10.1007/S00382-012-1587-6/FIGURES/13

Cheung HHN, Zhou W, Lee SM, Tong HW (2015) Interannual and interdecadal variability of the number of cold days in Hong Kong and their relationship with large-scale circulation. Mon Weather Rev 143:1438–1454. https://doi.org/10.1175/MWR-D-14-00335.1

Collins WJ, Lamarque J-F, Schulz M, Boucher O, Eyring V, Hegglin MI, Maycock A, Myhre G, Prather M, Shindell D, Smith SJ (2017) AerChemMIP: quantifying the effects of chemistry and aerosols in CMIP6. Geosci Model Dev 10:585–607. https://doi.org/10.5194/gmd-10-585-2017

Cui L, Shi J, Du H, Wen K (2017) Characteristics and trends of climatic extremes in China during 1959–2014. J Trop Meteorol 23:368–379. https://doi.org/10.16555/j.1006-8775.2017.04.003

Dawson A (2016) eofs: A library for EOF analysis of meteorological, oceanographic, and climate data. J Open Res Softw 4:14. https://doi.org/10.5334/JORS.122

Deng Y, Park TW, Cai M (2012) Process-based decomposition of the global surface temperature response to El Niño in boreal winter. J Atmos Sci 69:1706–1712. https://doi.org/10.1175/JAS-D-12-023.1

Deng Y, Park TW, Cai M (2013) Radiative and dynamical forcing of the surface and atmospheric temperature anomalies associated with the Northern annular mode. J Clim 26:5124–5138. https://doi.org/10.1175/JCLI-D-12-00431.1

Di Luca A, de Elía R, Bador M, Argüeso D (2020) Contribution of mean climate to hot temperature extremes for present and future climates. Weather Clim Extrem 28:100255. https://doi.org/10.1016/J.WACE.2020.100255

Dong S, Sun Y, Aguilar E, Zhang X, Peterson TC, Song L, Zhang Y (2018) Observed changes in temperature extremes over Asia and their attribution. Clim Dyn 51:339–353. https://doi.org/10.1007/S00382-017-3927-Z/FIGURES/9

Ebi KL, Bowen K (2016) Extreme events as sources of health vulnerability: drought as an example. Weather Clim Extrem 11:95–102. https://doi.org/10.1016/J.WACE.2015.10.001

Fan H, Hu X, Yang S, Choi YS, Lee YK (2021) Process-based analysis of relative contributions to the multi-model warming projection over East Asia. Clim Dyn 56:2729–2747. https://doi.org/10.1007/S00382-020-05614-7/FIGURES/11

Fischer EM, Knutti R (2015) Anthropogenic contribution to global occurrence of heavy-precipitation and high-temperature extremes. Nat Clim Change 5:560–564. https://doi.org/10.1038/nclimate2617

Fu D, Ding Y (2021) The study of changing characteristics of the winter temperature and extreme cold events in China over the past six decades. Int J Climatol 41:2480–2494. https://doi.org/10.1002/joc.6970

Gelaro R, McCarty W, Suárez MJ, Todling R, Molod A, Takacs L, Randles CA, Darmenov A, Bosilovich MG, Reichle R, Wargan K, Coy L, Cullather R, Draper C, Akella S, Buchard V, Conaty A, da Silva AM, Gu W, Kim GK, Koster R, Lucchesi R, Merkova D, Nielsen JE, Partyka G, Pawson S, Putman W, Rienecker M, Schubert SD, Sienkiewicz M, Zhao B (2017) The modern-era retrospective analysis for research and applications, version 2 (MERRA-2). J Clim 30:5419–5454. https://doi.org/10.1175/JCLI-D-16-0758.1

Gong Z, Feng G, Ren F, Li J (2014) A regional extreme low temperature event and its main atmospheric contributing factors. Theor

Appl Climatol 117:195–206. https://doi.org/10.1007/S00704-013-0997-7/FIGURES/12

Guan X, Gao Z, Huang J, Cao C, Zhu K, Wang J (2022) Speeding extreme cold events under global warming. Environ Res Lett 17:084012. https://doi.org/10.1088/1748-9326/ac8110

Ha KJ, Seo YW, Yeo JH, Timmermann A, Chung ES, Franzke CLE, Chan JCL, Yeh SW, Ting M (2022) Dynamics and characteristics of dry and moist heatwaves over East Asia. Npj Clim Atmos Sci 5:49. https://doi.org/10.1038/s41612-022-00272-4

Harris RMB, Beaumont LJ, Vance TR, Tozer CR, Remenyi TA, Perkins-Kirkpatrick SE, Mitchell PJ, Nicotra AB, McGregor S, Andrew NR, Letnic M, Kearney MR, Wernberg T, Hutley LB, Chambers LE, Fletcher MS, Keatley MR, Woodward CA, Williamson G, Duke NC, Bowman DMJS (2018) Biological responses to the press and pulse of climate trends and extreme events. Nat Clim Change 8:579–587. https://doi.org/10.1038/s41558-018-0187-9

Hersbach H, Bell B, Berrisford P, Hirahara S, Horányi A, Muñoz-Sabater J, Nicolas J, Peubey C, Radu R, Schepers D, Simmons A, Soci C, Abdalla S, Abellan X, Balsamo G, Bechtold P, Biavati G, Bidlot J, Bonavita M, De Chiara G, Dahlgren P, Dee D, Diamantakis M, Dragani R, Flemming J, Forbes R, Fuentes M, Geer A, Haimberger L, Healy S, Hogan RJ, Hólm E, Janisková M, Keeley S, Laloyaux P, Lopez P, Lupu C, Radnoti G, de Rosnay P, Rozum I, Vamborg F, Villaume S, Thépaut JN (2020) The ERA5 global reanalysis. Q J R Meteorol Soc 146:1999–2049. https://doi.org/10.1002/qj.3803

Hu X, Yang S, Cai M (2016) Contrasting the eastern Pacific El Niño and the central Pacific El Niño: process-based feedback attribution. Clim Dyn 47:2413–2424. https://doi.org/10.1007/s00382-015-2971-9

Hu X, Cai M, Yang S, Sejas SA (2018) Air temperature feedback and its contribution to global warming. Sci China Earth Sci 61:1491–1509. https://doi.org/10.1007/s11430-017-9226-6

Hu X, Fan H, Cai M, Sejas SA, Taylor P, Yang S (2020) A less cloudy picture of the inter-model spread in future global warming projections. Nat Commun 11:4472. https://doi.org/10.1038/s41467-020-18227-9

Hu X, Ma J, Ying J, Cai M, Kong Y (2021) Inferring future warming in the Arctic from the observed global warming trend and CMIP6 simulations. Adv Clim Chang Res 12:499–507. https://doi.org/10.1016/J.ACCRE.2021.04.002

Kong Y, Wu Y, Hu X, Li Y, Yang S (2022) Uncertainty in projections of the South Asian summer monsoon under global warming by CMIP6 models: Role of tropospheric meridional thermal contrast. Atmos Ocean Sci Lett 15:100145. https://doi.org/10.1016/J.AOSL.2021.100145

Lewis SC, King AD (2017) Evolution of mean, variance and extremes in 21st century temperatures. Weather Clim Extrem 15:1–10. https://doi.org/10.1016/J.WACE.2016.11.002

Lu J, Cai M (2009) A new framework for isolating individual feedback processes in coupled general circulation climate models. Part i: formulation. Clim Dyn 32:873–885. https://doi.org/10.1007/s00382-008-0425-3

McMichael AJ (2013) Globalization, climate change, and human health. N Engl J Med 368:1335–1343. https://doi.org/10.1056/NEJMRA1109341/SUPPL_FILE/NEJMRA1109341_DISCLOSURES.PDF

Melbourne J, Williams BF, Dalcanton JJ (2019) Changes in temperature extremes on the Tibetan Plateau and their attribution. Environ Res Lett 14:124015. https://doi.org/10.1088/1748-9326/AB503C

North GR, Bell TL, Cahalan RF, Moeng FJ (1982) Sampling errors in the estimation of empirical orthogonal functions. Mon Weather Rev 110:699–706

Park TW, Deng Y, Cai M (2012) Feedback attribution of the El Niño-Southern Oscillation–related atmospheric and surface temperature anomalies. J Geophys Res Atmos 117:D23101. https://doi.org/10.1029/2012JD018468

Raymond C, Horton RM, Zscheischler J, Martius O, AghaKouchak A, Balch J, Bowen SG, Camargo SJ, Hess J, Kornhuber K, Oppenheimer M, Ruane AC, Wahl T, White K (2020) Understanding and managing connected extreme events. Nat Clim Chang 10:611–621. https://doi.org/10.1038/s41558-020-0790-4

Ren Z, Yu Y, Zou F, Xu Y (2012) Quality detection of surface historical basic meteorological data. J Appl Meteorol Sci 23:739–747

Seo YW, Ha KJ, Park TW (2021) Feedback attribution to dry heatwaves over East Asia. Environ Res Lett 16:064003. https://doi.org/10.1088/1748-9326/abf18f

Song L, Wu R (2017) Processes for occurrence of strong cold events over Eastern China. J Clim 30:9247–9266. https://doi.org/10.1175/JCLI-D-16-0857.1

Song L, Wu R (2022) Different processes of occurrence of cold events over East Asia in El Niño and La Niña winters. Clim Dyn 58:31391–33154. https://doi.org/10.1007/S00382-021-06082-3

van der Wiel K, Bintanja R (2021) Contribution of climatic changes in mean and variability to monthly temperature and precipitation extremes. Commun Earth Environ 2:1. https://doi.org/10.1038/s43247-020-00077-4

Wang L, Chen W (2014a) The East Asian winter monsoon: re-amplification in the mid-2000s. Chinese Sci Bull 59:430–436. https://doi.org/10.1007/s11434-013-0029-0

Wang L, Chen W (2014b) An intensity index for the East Asian winter monsoon. J Clim 27:2361–2374. https://doi.org/10.1175/JCLI-D-13-00086.1

Wang L, Lu M-M (2016) The East Asian Winter Monsoon. In: The Global Monsoon System, pp 51–61. https://doi.org/10.1142/9789813200913_0005

Wang W, Yang S, Li Q, Zhang T, Jiang X (2023) Alternate modulations of ENSO and the Arctic Oscillation on winter extreme cold events in China. Atmos Res 282:106532. https://doi.org/10.1016/j.atmosres.2022.106532

Wen M, Yang S, Kumar A, Zhang P (2009) An analysis of the large-scale climate anomalies associated with the snowstorms affecting China in January 2008. Mon Weather Rev 137:1111–1131. https://doi.org/10.1175/2008MWR2638.1

Yu Y, Li Y, Ren R, Cai M, Guan Z, Huang W (2022) An isentropic mass circulation view on the extreme cold events in the 2020/21 Winter. Adv Atmos Sci 39:643–657. https://doi.org/10.1007/S00376-021-1289-2

Zhang T, Deng Y, Chen J, Yang S, Gao P, Zhang H (2022a) Disentangling physical and dynamical drivers of the 2016/17 record-breaking warm winter in China. Environ Res Lett 17:074024. https://doi.org/10.1088/1748-9326/ac79c1

Zhang X, Fu Y, Han Z, Overland JE, Rinke A, Tang H, Vihma T, Wang M (2022b) Extreme cold events from East Asia to North America in winter 2020/21: comparisons, causes, and future implications. Adv Atmos Sci 39:553–565. https://doi.org/10.1007/S00376-021-1229-1

Zhou W, Chan JCL, Chen W, Ling J, Pinto JG, Shao Y (2009) Synoptic-scale controls of persistent low temperature and icy weather over Southern China in January 2008. Mon Weather Rev 137:3978–3991. https://doi.org/10.1175/2009MWR2952.1

Zuo Z, Zhang R, Huang Y, Xiao D, Guo D (2015) Extreme cold and warm events over China in wintertime. Int J Climatol 35:3568–3581. https://doi.org/10.1002/JOC.4229

Springer